Determination of the energy-momentum densities of aluminium by electron momentum spectroscopy



1999 J. Phys.: Condens. Matter 11 3645

(http://iopscience.iop.org/0953-8984/11/18/302)

J. Phys.: Condens. Matter **11** (1999) 3645–3661. Printed in the UK PII: S0953-8984(99)01098-X

# Determination of the energy–momentum densities of aluminium by electron momentum spectroscopy

M Vos†, A S Kheifets†, E Weigold†, S A Canney‡, B Holm§, F Aryasetiawan‖ and K Karlsson¶

† Research School of Physical Sciences and Engineering, Institute of Advanced Studies, ANU, Canberra, A.C.T. 0200, Australia
‡ Electronic Structure of Materials Centre, Flinders University of South Australia, GPO Box 2100, Adelaide, S.A. 5001, Australia
§ Department of Applied Physics, Chalmers University of Technology and Göteborg University, S-412 96 Göteborg, Sweden
‖ Joint Research Centre for Atom Technology, Angstrom Technology Partnership, 1-1-4 Higashi, Tsukuba, Ibaraki 305, Japan
¶ Department of Natural Science, Hgskolan i Skövde, 541 28 Skövde, Sweden

Received 20 January 1999

**Abstract.** The energy-resolved momentum densities of thin polycrystalline aluminium films have been measured using electron momentum spectroscopy (EMS), for both the valence band and the outer core levels. The spectrometer used for these measurements has energy and momentum resolutions of around 1.0 eV and 0.15 atomic units, respectively. These measurements should, in principle, describe the electronic structure of the film very quantitatively, i.e. the dispersion and the intensity can be compared directly with theoretical spectral momentum densities for both the valence band and the outer core levels. Multiple scattering is found to hamper the interpretation somewhat. The core-level intensity distribution was studied with the main purpose of setting upper bounds on these multiple-scattering effects. Using this information we wish to obtain a full understanding of the valence band spectra using different theoretical models of the spectral function. These theoretical models differ significantly and only the cumulant expansion calculation that takes the crystal lattice into account seems to describe the data reasonably well.

## 1. Introduction

A large amount of information on the electronic structure of solids has been acquired over the past thirty years, both theoretically and experimentally. The vast majority of these theories used for the interpretation of experiments are in terms of effective one-particle models. Exchange and correlation effects are acknowledged, but are assumed to only modify the effective potential probed by the electrons. This potential is usually obtained from some form of the density functional theory.

A proper way of calculating one-particle excitation spectra is to use the Green function theory. Central to this theory is the spectral function describing the final state of the system in terms of momentum and energy after the sudden removal of an electron. These spectral functions show dispersing structures rather similar to those obtained in the effective one-particle theories. However, they differ in two important respects.

Firstly, the calculated dispersing structures have (except right at the Fermi level) a finite but significant width, i.e. lifetime broadening due to decay of the state created by the removal

0953-8984/99/183645+17$19.50  

of an electron. Secondly, they give a significant fraction of the intensity (about 25%) at energy/momentum values well away from the dispersing quasi-one-electron structures. These satellites are often referred to as intrinsic plasmons, and are rooted in the screening of the created hole by the system, and hence are related to the electron–electron correlations.

There is only limited experimental evidence to test these theories. Lifetime widths can be obtained from photoelectron spectroscopy. The satellites are probed by photoemission as well, but their intensity is superimposed on intensity from extrinsic satellites excited by the outgoing electron as it propagates to the surface. For aluminium, measured values of the intensity ratio of the intrinsic satellite to the core level range from 0.11 to 0.34 [1]. The valence band case is even more complicated, as the excitation cross section in photoemission depends strongly on the angular momentum of the initial state. Moreover, these measurements determine dispersion (binding energy versus crystal momentum) and do not resolve momentum densities directly.

The momentum density is probed by Compton scattering. It measures the projection of the momentum density of the target electrons on the scattering vector. If a series of different directions are measured, one can reconstruct the 3D momentum distribution. The effect of electron–electron correlation on the measured momentum distribution is a reduction in size of the discontinuity at the Fermi momentum as well as a tail extending the momentum distribution to larger values. There is currently a discrepancy between the size of the measured discontinuity and the theoretically predicted one [2, 3].

In Compton scattering a photon transfers a large amount of energy to a target electron. Due to the fact that this electron is not detected one measures the momentum density of the target electron projected on the scattering vector. Attempts are being made to fully resolve the momentum density by measuring the emerging electron in coincidence with the scattered photon. In these $(\gamma, \mathrm{e}\gamma)$ experiments multiple scattering becomes a problem. The ejected electron should not transfer momentum on its way out of the solid. This requires thin free-standing films. This technique is still under development [4, 5]. However, using photons, this seems to be as far as one can go. It does not seem feasible with the current techniques to obtain energy information as well as momentum information.

The Compton experiments rely on impulsive collisions. The ejected electron is assumed to have such a large energy that it leaves the system without further interaction with the $(N-1)$-electron system left behind. This approximation is generally expected to be quite good for energies of the ejected electron of 1 keV or more [6].

Instead of photons one can use electrons as the incoming particles. The interaction of an electron with the target is much stronger than that of the photon (Møller versus Klein–Nishina cross sections [5]), and the electrons can be conveniently analysed for both energy and momentum using electrostatic analysers. This makes resolution of energy and momentum simultaneously feasible, opening the possibility of completely measuring the (occupied part of the) spectral function. This technique is referred to as electron momentum spectroscopy (EMS) [7, 8]. EMS is an (e, 2e) experiment performed under conditions such that the plane-wave impulse approximation is valid, i.e. in the limit of high energy and momentum transfer.

However, the price that one pays is that in these EMS experiments, due to the stronger interaction of the electron with the target, multiple scattering is an even larger problem than in the $(\gamma, \mathrm{e}\gamma)$ case, even for the thinnest of films. Indeed, only a small fraction of coincidences are related to clean events (i.e. without multiple scattering). In this paper we examine how much information about the spectral function one can obtain in spite of these multiple-scattering effects, using aluminium as an example.

There are a number of favourable factors. Firstly, the interaction of keV electrons with a solid is relatively simple and well understood, and can be described to a certain extent in a semiclassical way as straight trajectories separated by elastic (with the ion cores) or inelastic

(with the electrons) collisions. The average separation of these collisions is described by the elastic and inelastic mean free path. In this way one can model fairly accurately the multiple-scattering effects and attempt to correct for them.

Secondly, we have to describe three quantities i.e. the intensity at a certain momentum/binding energy combination. As we will see, this is a very stringent test, i.e. no calculated spectral function gives a perfect fit to the data even if one tries to adjust some of the parameters such as the elastic and or inelastic mean free path, film thickness etc. The disagreement between experiment and theory can be due to imperfections in either one or both of them. This makes it a stringent test case, and it will be interesting to see whether developments in experimental and theoretical techniques will resolve these differences.

The remainder of the paper is organized as follows. In the next section we establish the connection between the spectral function and the measured (e, 2e) intensity for a free-electron gas. Subsequently we present the (e, 2e) measurement over a wide energy range and see how we can use the core levels to get some upper limits on the multiple-scattering effects. Finally we concentrate on the valence band and see how different calculations compare with the measurements.

## 2. The relation between EMS and the spectral function

Previously we have compared EMS results with band-structure calculations. For the case of aluminium this was done by Canney *et al* [9, 10]. Briefly one solves the electronic structure of the solid in terms of Bloch functions

$$\Psi_{\boldsymbol{k}} = \sum_{\boldsymbol{G}} c_{\boldsymbol{G}} \mathrm{e}^{(\boldsymbol{k}+\boldsymbol{G})\cdot\boldsymbol{R}}.$$

Each Bloch function has a well defined energy and contributes to the EMS intensity at this energy and at a momentum $\boldsymbol{k} + \boldsymbol{G}$ by an amount proportional to $|c_{\boldsymbol{G}}|^2$. In order to see what changes if we want to take correlation effects explicitly into account, we briefly review the theory of electron momentum spectroscopy in solids so that we can get some insight into the nature of the approximations made in comparing the EMS results with a spectral function.

One can think of EMS as a high-energy EELS (electron energy-loss spectroscopy) experiment with the measured intensity restricted by an additional coincidence requirement. In an EELS experiment an incoming electron (energy $E_0$, momentum $\boldsymbol{k}_0$) scatters from a target system containing $N$ electrons and emerges with energy $E_1$ and momentum $\boldsymbol{k}_1$. We use $\omega$ for the transferred energy ($\omega = E_0 - E_1$) and $\boldsymbol{k}$ for the transferred momentum ($\boldsymbol{k} = \boldsymbol{k}_0 - \boldsymbol{k}_1$).

In the first Born approximation, which is valid at high energies, the scattering cross section of an EELS experiment can be written as

$$\frac{\mathrm{d}\sigma}{\mathrm{d}\omega\,\mathrm{d}\Omega} = C_k \frac{k_1}{k_0} S(\boldsymbol{k}, \omega) \tag{1}$$

with $C_k$ a term that depends on the particle–particle interaction and the momentum transfer [11]. For electrons it can be written as (we use atomic units throughout)

$$C_k = \frac{4}{k^4} N. \tag{2}$$

where $N$ is the number of electrons in the system. (Here we assume that $1/k^4 \gg 1/k_1^4$). It is a constant for a given measurement geometry. The second term is determined by the electronic structure of the target. It describes the time dependence of the density–density correlations and can be written as

$$S(\boldsymbol{k}, \omega) = \frac{1}{2\pi N} \int_{-\infty}^{\infty} \mathrm{d}t\ \mathrm{e}^{\mathrm{i}\omega t} \langle \rho_{\boldsymbol{k}}(t) \rho_{-\boldsymbol{k}}(0) \rangle \tag{3}$$

with $\rho_k(t) \equiv e^{iHt}\rho_k e^{-iHt}$ and $\rho_k$ the Fourier transform of the electron density in coordinate space and $H$ the Hamiltonian of the $N$-electron system. Equation (1) is the central formula used in the interpretation of EELS experiments, and was first derived by Van Hove [12]. It assumes the sudden limit, i.e. no interaction between the outgoing (scattered) electron and the system left behind in an excited state.

In general a difference between an EMS experiment and a traditional EELS experiment is that the transferred momentum $k$ in the latter is much smaller than $k_0$, usually not more than 1 au. In EMS our aim is to measure momentum densities and thus we want to scatter from individual electrons. The size of the area from which we scatter is of the order of $1/k$. Thus in order to have these binary collisions we need large momentum transfer, perhaps even up to the maximum possible, $k_0/\sqrt{2}$.

In the case of high momentum transfer in a binary collision both the scattered and ejected electron can be approximated by a free electron. Thus for the final state we can write

$$|\alpha_N\rangle = |\boldsymbol{k}_2\alpha_{N-1}\rangle. \tag{4}$$

where $\boldsymbol{k}_2$ is the momentum of the ejected electron. This means that there is no interaction of the outgoing electrons with the $(N-1)$-electron system left behind, i.e. the reaction takes place in the sudden limit with respect to the ejected electron as well. Intuitively it is clear that the validity of this approximation is better for faster outgoing electrons.

Plane waves are the natural basis for a homogeneous (free-electron-like) system. (If one considered the crystal lattice, one would of course use Bloch waves.) Let $a_q$ and $a_q^\dagger$ be the annihilation and creation operators for an electron with momentum $\boldsymbol{q}$. Further define

$$a_q(t) = e^{iHt}a_q e^{-iHt}. \tag{5}$$

The electron density component $\rho_{\pm k}$ can be written as

$$\rho_k = \sum_q a_q^\dagger a_{q+k} \qquad \rho_{-k} = \sum_q a_{q+k}^\dagger a_q. \tag{6}$$

Using this notation we can write

$$\langle 0|\rho_k(t)\rho_{-k}(0)|0\rangle = \sum_{q,q'}\langle 0|a_q^\dagger(t)a_{q+k}(t)a_{q'+k}^\dagger(0)a_{q'}(0)|0\rangle. \tag{7}$$

Consider a system in the ground state $|0\rangle$. The momentum densities decrease rapidly above $k_F$ ($k_F$ being the Fermi momentum), even for an interacting electron gas. Those terms in the sum with either $q$ or $q' \gg k_F$ do not contribute to the sum, as these matrix elements are evaluated in the ground state. Thus for those terms that contribute, $|\boldsymbol{q}+\boldsymbol{k}| \gg k_F$, as we are interested in large values of the transferred momentum $k$, and we can write

$$\langle 0|a_q^\dagger(t)a_{q+k}(t)a_{q'+k}^\dagger(0)a_{q'}(0)|0\rangle = e^{-i\epsilon_{q+k}t}\langle 0|a_q^\dagger(t)a_{q'}(0)a_{q+k}(0)a_{q'+k}^\dagger(0)|0\rangle \tag{8}$$

Here

$$\epsilon_{q+k} = k^2/2 + (\boldsymbol{q}\cdot\boldsymbol{k}) + q^2/2$$

i.e. the time dependence of $a_{q+k}(t)$ (the ejected electron) is taken to equal that of a free electron with that momentum. $a_{q'+k}^\dagger$ creates an electron with momentum $\boldsymbol{q}'+\boldsymbol{k}$ with probability 1 as this level is unoccupied in the ground state due to the large magnitude of $\boldsymbol{k}$ (and the small magnitude of $\boldsymbol{q}'$). The matrix element is zero unless this electron is annihilated by $a_{q+k}$. This means that $\boldsymbol{q}' = \boldsymbol{q}$. Thus we are left with

$$\sum_{q,q'}\langle 0|a_q^\dagger(t)a_{q+k}(t)a_{q'+k}^\dagger(0)a_{q'}(0)|0\rangle = \sum_q\langle 0|a_q^\dagger(t)a_q(0)|0\rangle e^{-i\epsilon_{q+k}t}. \tag{9}$$

Substituting this back in equation (3), the familiar results of a Compton profile being measured in a high-momentum-transfer EELS experiment are obtained [13]. In our case we measure

the ejected electron as well. This means that we determine $\boldsymbol{q}+\boldsymbol{k}$, and hence instead of a summation over $\boldsymbol{q}$ in equation (9) only the term with $\boldsymbol{q}=\boldsymbol{k}_1+\boldsymbol{k}_2-\boldsymbol{k}_0$ contributes. The energy analysis of the ejected electron determines $\varepsilon_{\boldsymbol{q}+\boldsymbol{k}}$. Thus we can write the energy-resolved cross section of an (e, 2e) experiment using equation (3), equation (5) and equation (9) as

$$\frac{\mathrm{d}\sigma^4}{\mathrm{d}E_1\,\mathrm{d}E_2\,\mathrm{d}\Omega_1\,\mathrm{d}\Omega_2}=\left(\frac{1}{2\pi}\right)^5\frac{k_1k_2}{k_0}|V(k)|^2\int_{-\infty}^{\infty}\frac{\mathrm{d}t}{2\pi}\,\langle 0|a_{\boldsymbol{q}}^{\dagger}(t)a_{\boldsymbol{q}}(0)|0\rangle\mathrm{e}^{-\mathrm{i}(E_0-E_1-E_2)t}. \tag{10}$$

Here $V(k)=4\pi/k^2$ is the Fourier transform of the Coulomb potential. Note that the integral is a real quantity, as the contribution at $t$ is the complex conjugate of the contribution at $-t$.

In the sudden approximation there is no interaction after the collision between the system and the emerging electrons. The measured energy $\epsilon=E_0-E_1-E_2$ is thus the energy of the state created at $t=0$ with momentum $\boldsymbol{q}$. Now compare this expression with the definition of the (retarded) Green's function:

$$\begin{aligned}G^-(\boldsymbol{q},t)&=-\mathrm{i}\Theta(t)\langle 0|a_{\boldsymbol{q}}^{\dagger}(t)a_{\boldsymbol{q}}(0)|0\rangle\\ G^-(\boldsymbol{q},\epsilon)&=-\mathrm{i}\int_0^{\infty}\langle 0|a_{\boldsymbol{q}}^{\dagger}(t)a_{\boldsymbol{q}}(0)|0\rangle\mathrm{e}^{-\mathrm{i}\epsilon t}\,\mathrm{d}t\end{aligned} \tag{11}$$

with $\Theta(t)=0$ for $t<0$ and 1 for $t>0$. $G^-(\boldsymbol{q},\omega)$ is complex. However, from the structure of these equations it is clear that this function is closely related to the (e, 2e) cross section:

$$\frac{\mathrm{d}\sigma^4}{\mathrm{d}E_1\,\mathrm{d}E_2\,\mathrm{d}\Omega_1\,\mathrm{d}\Omega_2}=\frac{1}{(2\pi)^5}\frac{k_1k_2}{k_0}|V(k)|^2(-\pi)^{-1}\,\mathrm{Im}\,G^-(\boldsymbol{q},\epsilon). \tag{12}$$

The same result was obtained by D'Andrea and Del Sole, in the context of (e, 2e) measurements of reconstructed surfaces [14]. This is the central equation for the interpretation of the EMS results of a many-electron interacting system. The measured intensity is proportional to a constant which depends on the kinematics of the experiment and the imaginary part of the one-particle Green's function (spectral function). Thus instead of comparing the EMS results simply with the modulus of the square of the wave function in momentum space, as is done in single-particle theories, we have to compare the EMS results with the spectral function which is a key element of the many-body formalism.

This relation between the spectral function and the measured intensity is a direct consequence of the impulse approximation. The above derivation is given mainly to bring out two important differences between photoemission experiments and these electron scattering experiments. In EMS there are no different matrix elements for different electrons (s, p etc). Also the measurement of dispersion does not rely on the crystal periodicity, as crystal momentum does not appear in the above derivation. The latter reason makes EMS a probe that can test jellium-type calculations of free-electron-like materials such as aluminium, as the crystal potential is not an essential part of the excitation process.

## 3. Spectral functions for aluminium

In this paper we use four different spectral functions. First we use a linear muffin-tin orbital (LMTO) calculation of the aluminium band structure based on the local density approximation of the density functional theory (model A). In this model correlation effects are assumed to affect only the effective one-particle Hamiltonian. This calculation was used in the previous paper describing these experiments [9]. As our sample is polycrystalline, the results of the calculation are averaged over all directions.

As this is a one-particle theory, there is no lifetime broadening of the Bloch states. It was found in [9] that if empirical lifetime broadening was added (taken from Levinson *et al* [15]),

it could describe the data from the Fermi level to the bottom of the band quite well, but failed at higher binding energies. Thus the empirical lifetime broadening is included again in model A.

As much as 30 years ago it was predicted theoretically that the sudden removal of an electron from a free-electron gas may result in the excitations of plasmons in the system. The final state then has a larger energy, not just the binding energy of the electron removed from a free-electron gas, and hence there are satellites at higher binding energy in the spectrum. The simplest model that abandons the effective one-particle assumption and incorporates these satellites is the $G_0W$ calculation as described by Lundqvist [16]. This is our model B. This model neglects the lattice (it is a jellium model). Satellites appear now at higher binding energies and the quasi-particle part of the spectral function has lifetime broadening. However, it is known from photoemission data that the satellite position predicted by model

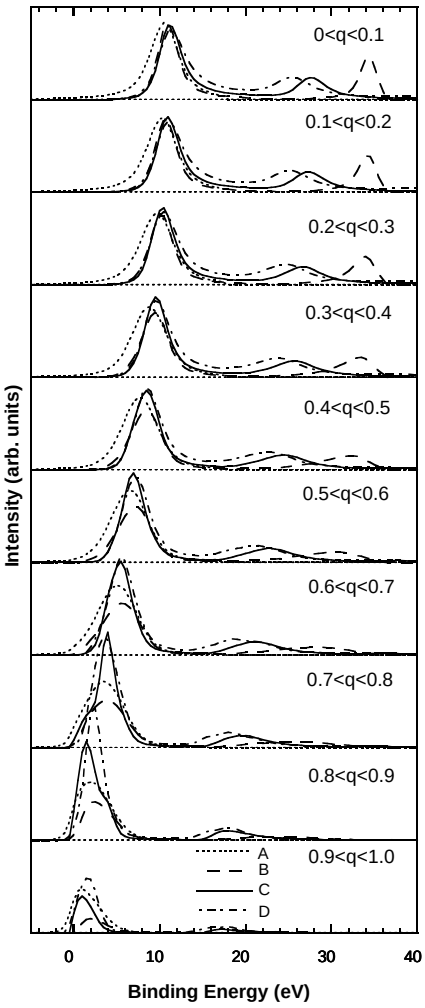


**Figure 1.** Four different spectral functions of aluminium as derived from the four different theories A–D as described in the text. The theories are convoluted with the experimental energy (1.5 eV) and momentum resolution (0.15 au). They are all normalized to equal height of the quasi-particle peak at zero momentum.

B (at $\simeq 1.5 \times$ the plasmon energy) is not supported by experiment. The model is reproduced here for completeness.

The third model (model C) is a more recent calculation using cumulant expansion techniques [17–21] as described in references [22, 23]. For reasons that will be apparent when we compare our theoretical model with the experimental spectrum, we have used the cumulant expansion in a *non*-self-consistent manner. Using a cumulant expansion scheme, the problem with the satellite energy seems to be rectified. It is again a model that neglects the crystal lattice.

Finally, model D is the result of a cumulant expansion calculation including the crystal lattice. Again it is averaged over all directions. Calculations were done for 30 different $k$-points in the first Brillouin zone.

Near the Fermi level the spectral function is sharply peaked. The energy step size in calculation C and the coarseness of the $k$-grid in calculation D seem to affect the area of the peak height obtained near the Fermi level somewhat. The four different theories, after convolution with the experimental energy (1.5 eV) and momentum resolution (0.15 au), are plotted in figure 1 for momentum values from 0 to 1 au. Binding energies in this and the following figures are relative to the Fermi level. In spite of our modest resolutions, the differences between the different models should be well resolved with the present spectrometer.

## 4. Experimental procedure

The experimental procedure was described extensively in reference [9]. In brief, we evaporated a thin aluminium layer ($\simeq$40 Å) onto a free-standing carbon membrane ($\simeq$60 Å thick). The sample was transferred under UHV (ultra-high vacuum) to the EMS spectrometer and measured for a period of 2–3 days. The EMS spectrometer uses an asymmetric geometry, with a relatively slow ejected electron (20 keV incoming beam, 18.8 keV fast (scattered) outgoing electron, 1.2 keV slow (ejected) outgoing electron). Due to a relatively low energy of the slow electron the experiment is mainly sensitive to one side of the sample (the one covered with aluminium). For events occurring at large depths (in the carbon layer) the probability of the slow electron escaping without elastic and/or inelastic scattering is extremely small. In no case did we observe a clear signature of the carbon layer in the spectra. Of course, (e, 2e) events occurring in the carbon substrate can contribute to the rather structureless background due to multiple scattering. Their contribution to the spectrum decreases due to the small mean free path for both elastic and inelastic scattering of the slow electron created during the (e, 2e) events.

As we will discuss later, the core levels show some indication of the presence of the initial stages of the oxidation of aluminium. In order to show that the contributions of either carbon and/or aluminium oxide are small, we present in figure 2 a spectrum of Al, $Al_2O_3$ and amorphous carbon, both at zero momentum and at a relatively high momentum (near 1.5 au). All energies are relative to the Fermi level. The aluminium spectrum does not extend far beyond 1 au (for aluminium $k_f = 0.97$ au). Much of the intensity measured at higher momentum values is due to (e, 2e) events with additional elastic scattering of the incoming and/or outgoing electrons, and hence it has no clear structure. Both the $Al_2O_3$ and the amorphous C spectra extend to larger momenta. If a substantial amount of either of these spectra were to be present in the measured Al valence band spectrum, it would be visible at high momentum. Multiple scattering in the carbon layer will however influence the shape of the background of the Al valence band. These processes are included in the Monte Carlo simulations, to be discussed later. More details on the oxidation of Al, as seen by EMS, can be found in [24] and on EMS of amorphous carbon in [25].

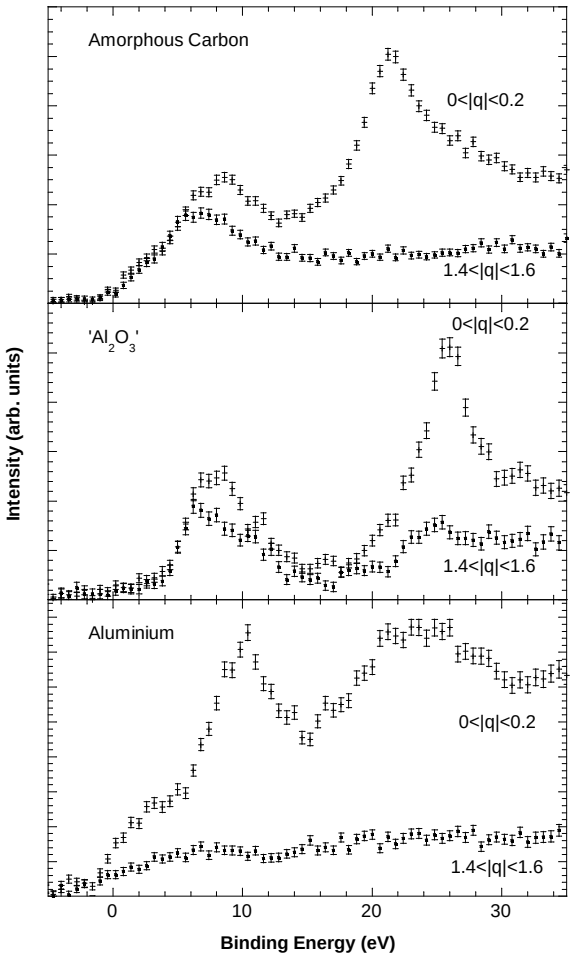


**Figure 2.** The spectra of amorphous carbon, aluminium oxide and aluminium for momentum values near zero and near 1.5 au. The distinct features in the aluminium spectra extend only up to 1.0 au and from these spectra it is clear that neither aluminium oxide or carbon contributes significantly to the aluminium spectra.

## 5. Experimental results

### *5.1. Introduction*

In figure 3 (left-hand panel) we show the experimental EMS data over a binding energy range of 140 eV. The data show the measured intensity integrated over different momentum ranges. For small momenta (<0.5 au) the main peak is in the valence band region, although other sharp features (namely the 2s and 2p core levels) are also present at larger binding energies. At higher momenta the valence band features become less pronounced, whereas the intensity of the core levels persists. In this plot we also show the intensity as predicted by a single-particle theory, without multiple scattering. For the theory the valence band structure was obtained from an LMTO calculation with empirical lifetime broadening (model A), whereas the core-level momentum distributions were taken to be equal to those for the atomic case and the

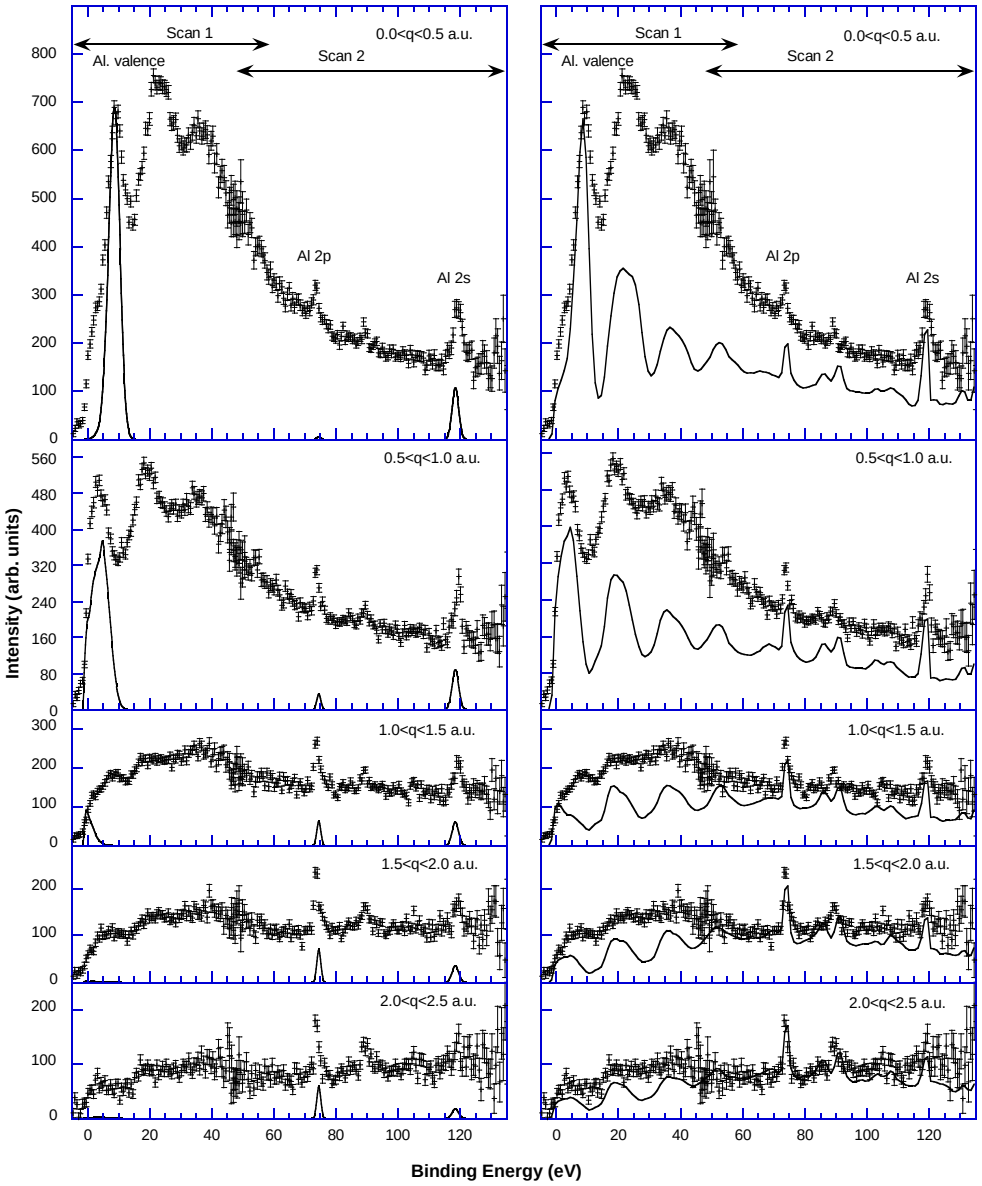


**Figure 3.** A scan for an aluminium film over a wide energy range that includes both the valence band and the outer core levels. The data are integrated over five momentum ranges, as indicated. In the left-hand panel we compare the data with a theory (LMTO calculation) that does not include multiple-scattering effects. In the right-hand panel the theoretical intensity is corrected approximately for multiple scattering.

binding energies of the core levels were taken from photoemission data. The intensity ratio of the core level and valence band is, however, not a free parameter since all the wave functions are normalized to the total number of electrons in that level. The calculations were convoluted with the experimental energy and momentum broadening. Additional lifetime broadening was added for the 2s level to obtain agreement with the experimental width of 2 eV FWHM. (For

the 2p level, lifetime broadening is not resolved.)

In all cases there is a sharp feature in the measured spectrum at the positions predicted by the calculations. However, it is obvious from this plot that the large majority of events are not directly related to either the core levels or the valence band. In these cases the (e, 2e) event was not the only interaction of the electrons with the solid. Inelastic scattering has occurred as well, and has shifted the intensity to lower binding energies. Indeed the highest peaks in the lower-momentum ranges are not in the valence band region, but occur just below the valence band region.

It is interesting to note that in EMS the valence band dominates the spectrum at low momentum. As these valence wave functions are extended in real space they are confined to the low-momentum region in momentum space, and hence have a relatively high intensity at low momentum. The much more localized core levels are confined in real space, and thus extended in momentum space, and consequently have smaller intensities in the experiment. The ratio of the valence band to core-level intensity in the experiment is of the same order as the calculated one. The ratio of the valence to core levels is completely different for EMS compared to the one obtained in XPS (x-ray photoelectron spectroscopy). In the latter case the core levels are by far the most intense features. This fact reflects the great differences in the excitation processes of the two techniques.

Thus, although there is a clear signature of the spectral momentum densities in these plots, it is also clear that the majority of events are not directly related to it. In these cases additional scattering occurred for either the incoming or outgoing electron trajectories. These effects can be modelled using semi-empirical models of electron propagation in solids. We carried out Monte Carlo simulations as described by Vos and Bottema [26]. Briefly, their method uses inelastic and elastic mean free paths for the distribution of the elastic and inelastic collisions. The magnitudes of the deflections due to elastic collisions are derived from the cross section of elastic scattering of an electron from an atom. The energy loss is set equal to the plasmon energy (with a spread around the mean corresponding to the experimentally determined width).

In the present simulations we included surface plasmons as well. The probability of surface plasmon creation can be obtained from theory (see e.g. Stern and Ferrel [27], or the summary given by Egerton [28]). However, the appearance of the surface plasmon component is coupled to a reduction of the bulk plasmon component. This means that the excitation probability of the bulk plasmon near the surface is smaller, i.e. its mean free path should increase near the surface. This is not easily implemented in our Monte Carlo code and was not attempted. Instead we used bulk plasmon creation rates everywhere, and hence overestimate the bulk plasmon creation rate slightly.

The results are shown in figure 3 (right-hand panel). The simulation was normalized to the experiment using the same normalization factor for all five momentum intervals, obtained by setting the valence peak height equal to the experimental one for the lowest momentum interval. Clearly the theory together with the simulations predicts intensity all the way down to high binding energies. However, the measured intensity is still larger than the calculated intensity, especially for small momentum values, and for binding energies between 15 and 60 eV.

### *5.2. Core levels*

It is clear that even after including multiple scattering with Monte Carlo simulations, the agreement with the measurement is still poor. Let us now focus on the 2p core level. This is the sharpest structure (in energy) in the experiment, with a momentum distribution which is supposedly very close to the atomic one. These results are shown in figure 4. In the central

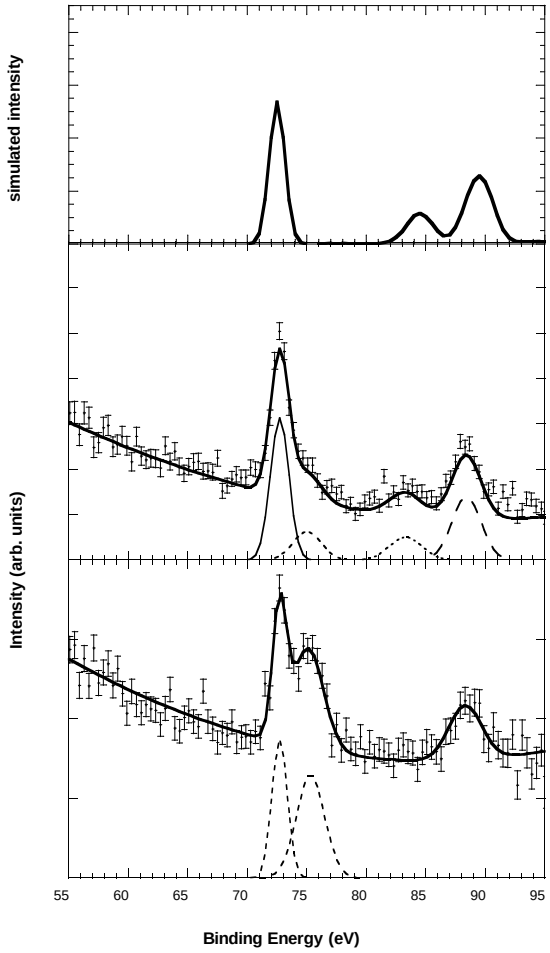


**Figure 4.** In the central panel we show the Al 2p core level as measured by EMS. The intensity was integrated from 0 to 2.5 au of momentum. Four different contributions can be distinguished with increasing binding energy: the main component, a contamination-related component and the surface and the bulk plasmon components. The top panel shows the 2p intensity, as predicted by the Monte Carlo simulations as discussed in the text. The lower panel shows the result of exposure of the aluminium film to 600 L of $O_2$.

panel we show the experimental data. These coincidence experiments have rather low count rates and the data shown are the result of a two-day measurement. In spite of a vacuum below $1.0 \times 10^{-10}$ Torr there is still a tail on the high-binding-energy side of the 2p peak. A small part of the intensity on the high-binding-energy side will be due to the non-resolved spin–orbit splitting and the asymmetry of the Doniach–Sunjic lineshape, which was not incorporated in the fit. However, for the largest part it will be due to some oxidation of the surface. The exact area of this contribution is difficult to estimate, but for the fit shown it is $\simeq$25% of the main line, which we consider as an upper limit.

It should be noted that in the case of the graphite 1s core level a very similar tail, extending to higher binding energies, was observed [29]. This is the only other core level that has been studied in detail with the current spectrometer. Thus the impurity satellite could as well be an

artefact of the spectrometer.

In the lowest panel we show the effect of purposely exposing a fresh Al film, prepared in an identical manner, to 600 L of oxygen. In this case the effects of oxidation are much more pronounced. Full details of a systematic study of the oxidation of an aluminium surface by EMS were given by Canney *et al* [24].

The main 2p structure has a width of 1.5 eV. The spin–orbit splitting ($\simeq$0.4 eV) is thus not resolved. However, it sets an upper limit of the resolution of the spectrometer (and stability over a two-day period) of about 1.3 eV. There is no reason that this resolution should not apply to the valence band data, as they are taken under identical circumstances. However, to be somewhat conservative we use the value of 1.5 eV for our assumed valence band resolution.

There are two more structures visible in figure 4. One is 15.6 eV away from the main line, hence related to the plasmon satellite, and has 69% of the intensity of the main line. The other is shifted by 10.6 eV, which corresponds to the surface plasmon and it has 28% of the intensity of the main line.

In order to obtain the intensities of the different components we fitted the background with a second-order polynomial. This background above the Al 2p level can only have its origin in (e, 2e) events with the valence band (in the carbon or aluminium layer) plus additional energy-loss events. We would like to point out that there is an intrinsic danger in this procedure. If there are very broad satellites to the core level then we may incorporate these features inadvertently in the background originating from the valence electrons.

Next we want to use the core-level intensity obtained as a test of the validity of the Monte Carlo simulations. In the simulations we can 'turn off the valence band' contribution to the measured spectrum (and at the same time change nothing in the elastic and/or inelastic scattering behaviour). We obtain then an intensity of the Al 2p core level and its associated plasmon and surface plasmon. The result of this simulation is shown in the top panel of figure 4.

In discussions of the plasmon intensity of core levels in photoemission experiments, one usually uses the three-step model, i.e. one assumes that it is possible to separate the excitation step from the propagation to the surface and subsequent escape steps. It is then possible, in principle, to distinguish between intrinsic and extrinsic plasmons, i.e. those created during excitation and those created during subsequent propagation of the photoelectron to the surface. In the above analysis we do not include intrinsic plasmons. One should thus consider the simulations to give only an upper bound of the contributions of extrinsic loss processes. Values of the creation rates of intrinsic plasmons as compiled by Hüfner for the Al 2p core level range from 0.11 to 0.34 relative to the main line [1]. The reduction in the bulk plasmon creation due to the surface, which is not taken into account in the simulations, is theoretically estimated to be close to half the creation rate of the surface plasmon [30]. The reasonable agreement obtained in the simulation could thus be due to the fact that the contribution of the intrinsic plasmon, and the reduction of the extrinsic bulk plasmon, due to surface effects, are of similar magnitude.

Besides giving a good description of the energy spectra, the simulations also have to describe the observed momentum distributions. For the Al 2s and 2p lines this is shown in figure 5. First the spectra were integrated over a large momentum range. Then the main line was fitted with one Gaussian component only. The energy positions and widths of the peaks were determined and subsequently kept fixed. The spectra were then fitted over smaller momentum intervals, with only the shape of the background and the peak height allowed to vary. The resulting intensities showed a local minimum for the 2p level at zero momentum, whereas the 2s level has maximum intensity at zero momentum. The (atomic) Al 2p wave function itself has a node at zero momentum, and hence the atomic 2p density is zero at zero momentum (solid curves in figure 5). The residual intensity of the 2p level at zero momentum

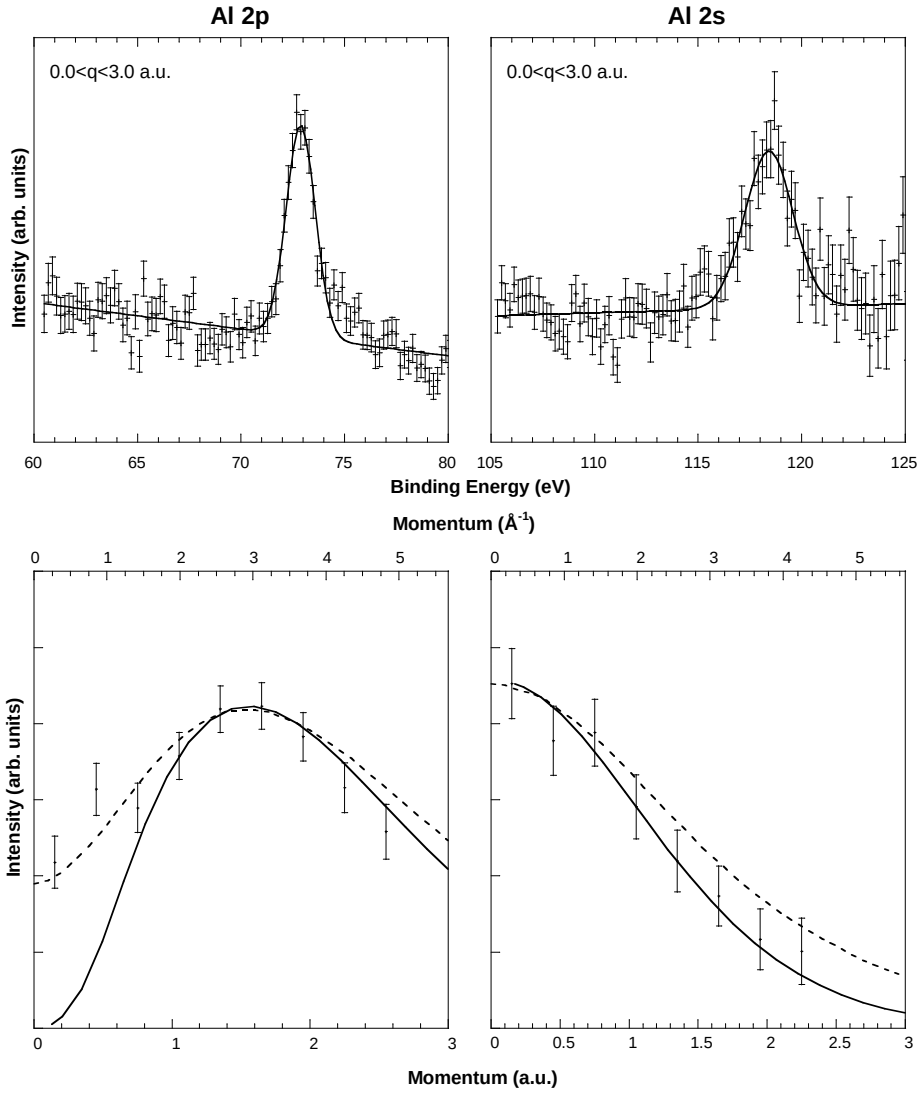


**Figure 5.** In the top two panels we show the Al 2p and Al 2s levels fitted with one Gaussian component. The position and width of this Gaussian was kept fixed and was used to determine the peak area of these lines as a function of momentum (error bars, lower two panels). The atomic 2p and 2s momentum densities are each indicated with a solid curve; the expected intensity based on the atomic momentum densities and an estimate of the effects of multiple scattering are indicated by the dashed curves.

cannot be explained by finite momentum resolution. Monte Carlo simulations as described above seem to predict the observed shapes fairly well, as is shown by the dashed curves. The measured intensity of the 2p level near zero momentum appears thus to be an effect of elastic scattering (i.e. the incoming and/or one of the outgoing electrons was deflected by an ion core, causing the wrong $\boldsymbol{q}$-value to be inferred from the momentum conservation equation).

Thus the core-level spectra seem to be described reasonably well, if we correct for multiple scattering, both in energy and momentum space. If anything, the Monte Carlo simulations

overestimate the aluminium plasmon-loss peak, as the current analysis does not take into account the possible existence of intrinsic plasmons.

### *5.3. The valence band*

We now return to the valence band results. They differ, of course, from those for the core levels in that the binding energy depends on momentum. This dispersion is well described by the band-structure calculations, which are now done routinely even for complicated solids. Our band-structure calculations are linear muffin-tin orbital (LMTO) calculations, using the atomic sphere approximation (model A). As our sample is polycrystalline, the results of the calculation have to be averaged over all directions. It was found by Canney *et al* [9] that the spherically averaged calculations were in good agreement with the experiment in the near-valence-band region, but that they underestimate the intensity at higher binding energies, even after inclusion of multiple-scattering effects [9]. The dispersing structure was, within experimental error, indistinguishable from a free-electron parabola—i.e. aluminium, as far as our experiment is concerned, seems to be a good example of an electron gas [9]. However, the intensity at large binding energies was underestimated by this approach.

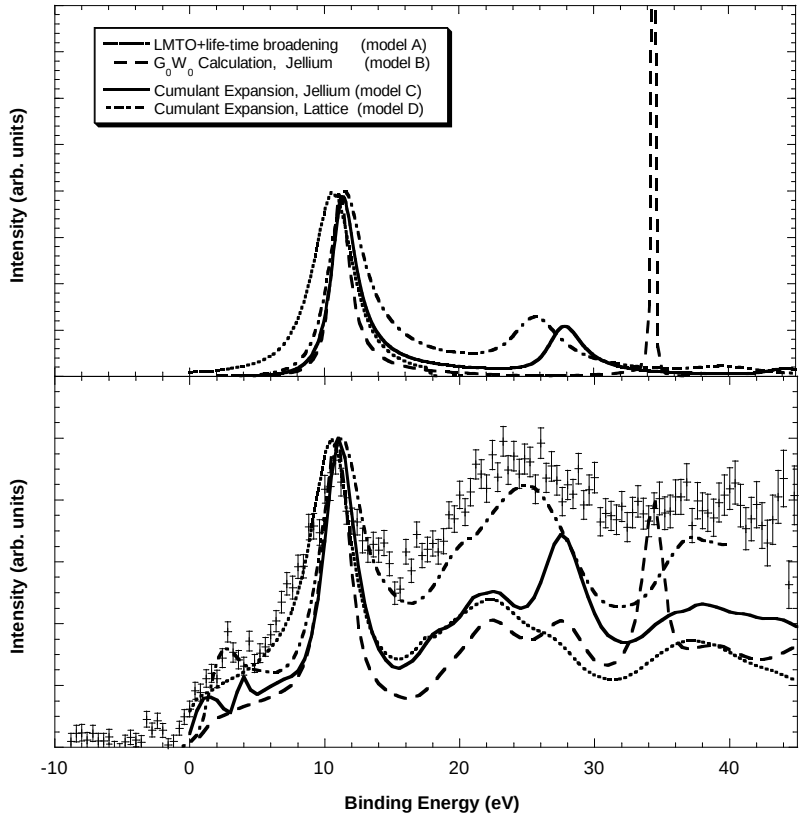


**Figure 6.** The valence band of aluminium for zero momentum. In the top panel we show the spectral function for zero momentum for the different theories as indicated. After including the same multiple-scattering effects as for the core level, we obtained the curves in the lower panel as a theoretical estimate of the measured intensity (error bars). All have been normalized to the same quasi-particle peak height at $\varepsilon \simeq 11$ eV.

This was the reason for the use of models B to D for comparison with our experiment, in the hope that these more sophisticated theories will give a better description of the experiment. First we plot again the spectral function at zero momentum (but now without broadening due to finite energy and momentum resolution) at $\boldsymbol{q} = \mathbf{0}$ (figure 6, upper panel).

As lifetime broadening is an essential component in these many-body theories, let us first compare the width of the quasi-particle peak as a function of binding energy. The empirical broadening is larger than the one obtained from theories. Canney *et al* [9] found that the empirical lifetime broadening based on the measurement of Levinson *et al* [15] described our experimental data very well. Near $\boldsymbol{q} = \mathbf{0}$ the assumed broadening was 3.5 eV FWHM. The theoretical spectral function has a width near $\boldsymbol{q} = \mathbf{0}$ of 1.7 eV for model B [16] and 2.4 eV for model C [23], whereas model D is closest to the empirical values (about 3 eV). Thus the

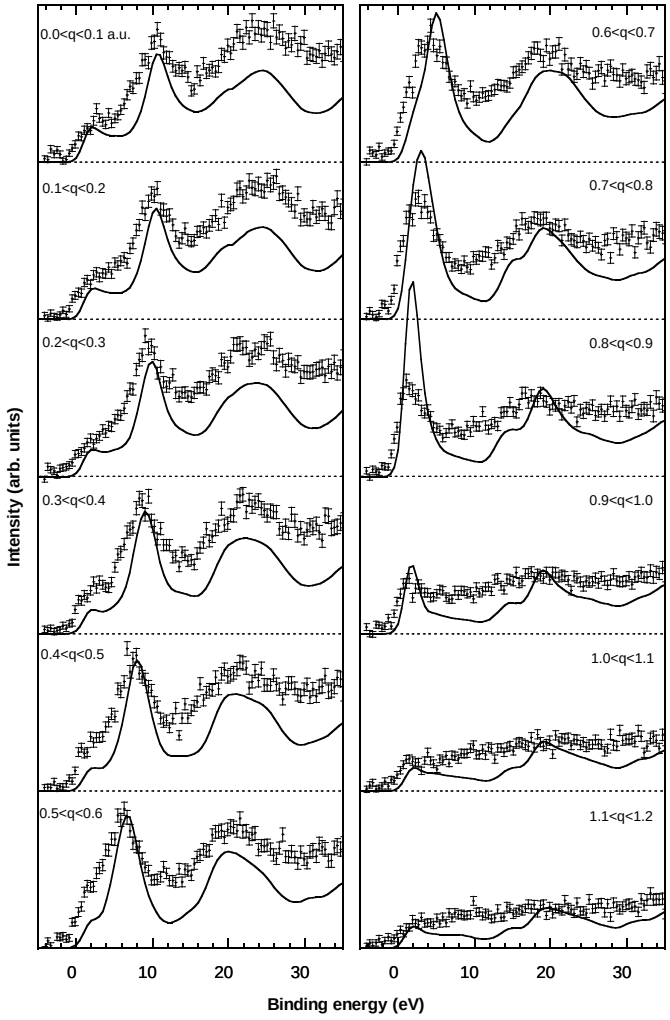


**Figure 7.** A comparison of the experimental data (error bars), for the momentum intervals as indicated and with the result of the Monte Carlo simulation using the spectral function based on the cumulant expansion, including the crystal lattice (model D) (solid curves).

crystal lattice (included in model D but not in model C) seems to increase the quasi-particle width significantly and also appears to affect the exact position of the intrinsic satellite.

In figure 6 (lower panel) we show the simulated experiment, based on these theories and using Monte Carlo simulations for the multiple scattering. All parameters of the simulations were identical to those describing the core levels. The simulated intensities were normalized, for convenience, to equal peak height at the quasi-particle peak. As expected, the quasi-particle peaks are too narrow for the jellium theories (models B and C) and slightly too narrow for model D. The $G_0W_0$ calculation (model B) predicts a sharp peak at 34 eV for which there are no indications in the experiment. The cumulant expansion theory predicts a peak near 27 eV binding energy, at somewhat higher binding energy and more pronounced than that found in the experiment. The separation of the satellite from the quasi-particle peak is very close to the plasmon energy here ($\simeq$15.5 eV) and therefore extrinsic and intrinsic losses combine to a well defined peak in the simulations. The general shape of model D (cumulant expansion including the lattice) agrees best with the experiment. Due to the larger width of the quasi-particle peak (compared to those found from models B and C) the intensity at high binding energy approaches the quasi-particle peak height. Also, due to the fact that the intrinsic satellite appears at a slightly lower energy than the plasmon satellite, extrinsic and intrinsic satellites combine to a rather broad feature, very much as in the experiment.

To get an impression of the overall performance of model D, not only for $\boldsymbol{q} = \mathbf{0}$, we plot the results of the simulations over a whole series of momentum values (figure 7). As the occupied states of Al extend outside the first Brillouin zone, but the calculations were done within the reduced zone, the resulting spectra for momenta near the Fermi wave vector are less reliable. The overall agreement, especially up to 0.8 au, is surprisingly good. The general shape of the spectra is reproduced nicely.

## 6. Conclusions

In this paper we investigated the energy-resolved momentum densities for both the core level and the valence band of aluminium. There seems to be a clear difference between the two parts of the spectrum. For the core level the plasmon-related satellites appear less intense than the main peak, whereas for the valence band part the intensity is as high in the plasmon-loss area as for the valence band itself. This conclusion is evident from the raw data, and thus does not rely on the analysis of the multiple-scattering contributions.

The simulations seem to give a reasonable description of the core-level region. Only the cumulant expansion theory, taking the lattice into account (model D), gives an adequate description of the measured valence band. Thus both electron–electron correlation and the lattice have to be considered to get a good description of the measurement. Surprisingly the measurement is not sensitive for the crystal lattice as far as the dispersion of the quasi-particle theory is concerned (it cannot distinguish it from a free-electron parabola for these polycrystalline samples) but the lattice seems to have a significant effect on the width of the quasi-particle peak. Also the fact that in model D the maximum in the satellite intensity is separated from the quasi-particle peak by less than the plasmon energy seems to be supported by the experiment. A similar broadening of the quasi-particle peak was found for Na (compare [23] (without a lattice) and [22] (with a lattice)).

A slight further improvement of the agreement would be obtained if the lifetime broadening in model D was slightly larger. However, given the purity of the sample and the approximate nature of the multiple-scattering simulations, the level of agreement seems quite satisfactory.

EMS seems to be an excellent probe for testing the calculations of spectral functions, especially if multiple-scattering effects can be reduced. This is possible by increasing the

energy of the incoming and outgoing electrons, which leads to an increase in the mean free path (at the expense of the cross section of the process). A high-energy spectrometer is currently under construction at the Australian National University.

## Acknowledgments

The experimental work at Flinders University was done at a Special Research Centre funded by the Australian Research Council. We acknowledge the contribution of the entire staff of the Centre to the work described here. BH acknowledges a post-doctoral fellowship at the materials and surface group at Chalmers/GU.

## References

[1] Hüfner S 1995 *Photoelectron Spectroscopy* (Berlin: Springer) ch 4
[2] Schülke W, Statz G, Wohlert F and Kaprolat A 1996 *Phys. Rev.* B **54** 14 381
[3] Králik B, Delaney P and Louie S G 1998 *Phys. Rev. Lett.* **80** 4253
[4] Kurp F F, Tschentscher Th, Schulte-Schrepping H, Schneider J R and Bell F 1996 *Europhys. Lett.* **35** 61
[5] Kurp F F, Vos M, Tschentscher Th, Kheifets A S, Schneider J R, Weigold E and Bell F 1997 *Phys. Rev.* B **55** 5440
[6] McCarthy I E and Weigold E 1991 *Rep. Prog. Phys.* **54** 789
[7] Dennison J R and Ritter A L 1996 *J. Electron Spectrosc. Relat. Phenom.* **77** 99
[8] Vos M and McCarthy I E 1995 *Rev. Mod. Phys.* **67** 713
[9] Canney S A, Vos M, Kheifets A S, Clisby N, McCarthy I E and Weigold E 1997 *J. Phys.: Condens. Matter* **9** 1931
[10] Canney S A, Kheifets A S, Vos M and Weigold E 1998 *J. Electron Spectrosc. Relat. Phenom.* **88–91** 247
[11] Schnatterley S E 1979 *Solid State Physics* vol 34 (New York: Academic) p 275
[12] Van Hove L 1954 *Phys. Rev.* **95** 249
[13] Platzman P M and Tzoar N 1965 *Phys. Rev.* **139** A410
[14] D'Andrea A and Del Sole R 1978 *Surf. Sci.* **71** 306
[15] Levinson H J, Greuter F and Plummer W 1983 *Phys. Rev.* B **27** 727
[16] Lundqvist B I 1968 *Phys. Kondens. Mater.* **7** 117
[17] Langreth D C 1970 *Phys. Rev.* B **1** 471
[18] Bergersen B 1973 *Can. J. Phys.* **51** 102
[19] Hedin L 1980 *Phys. Scr.* **21** 477
[20] Almbladh C-O and Hedin L 1983 *Handbook on Synchroton Radiation* vol 1, ed E E Koch (Amsterdam: North-Holland) p 686
[21] Gunnarsson O, Meden V and Schönhammer K 1994 *Phys. Rev.* B **50** 10 462
[22] Aryasetiawan F, Hedin L and Karlsson K 1996 *Phys. Rev. Lett.* **77** 2268
[23] Holm B and Aryasetiawan F 1997 *Phys. Rev.* B **56** 12 825
[24] Canney S A, Vos M, Kheifets A S, Guo X, McCarthy I E and Weigold E 1997 *Surf. Sci.* **382** 241
[25] Vos M, Storer P J, Cai Y Q, McCarthy I E and Weigold E 1995 *Phys. Rev.* B **51** 1866
[26] Vos M and Bottema M 1996 *Phys. Rev.* B **54** 5946
[27] Stern E A and Ferrel R A 1960 *Phys. Rev.* **120** 130
[28] Egerton R F 1986 *Electron Energy Loss Spectroscopy* (New York: Plenum)
[29] Canney S A, Brunger M J, McCarthy, I E, Storer P J, Utteridge S, Vos M and Weigold E 1997 *J. Electron Spectrosc. Relat. Phenom.* **83** 65
[30] Ritchy R H 1957 *Phys. Rev.* **120** 130